



Research Article

Micro-hardness and wear behavior of AA2014/Al₂O₃ surface composite produced by friction stir processing

Shalok Bharti¹  · Nilesh D. Ghetiya¹  · Kaushik M. Patel¹ 

Received: 9 July 2020 / Accepted: 23 September 2020 / Published online: 3 October 2020
© Springer Nature Switzerland AG 2020

Abstract

The present study aimed to improve the micro-hardness and wear properties of AA2014 aluminum alloy. Surface composite of AA2014 was produced using Al₂O₃ as reinforcement by friction stir processing (FSP) technique. FSP was performed by using a constant traverse speed of 40 mm/min and two rotating speeds of 1000 and 1400 rpm. After FSP, the average grain size of AA2014 was reduced from 21.9 μm in base material to 9.2 μm in FSP with a rotating speed of 1000 rpm and 3.8 μm in FSP with rotating speed of 1400 rpm. Optical microscopy showed that the Al₂O₃ reinforcement particles were distributed homogeneously in AA2014 after FSP. The micro-hardness test showed that the hardness property in AA2014/Al₂O₃ surface composite was improved after FSP and was increased with an increase in rotating speed. The micro-hardness was improved by 30% after FSP. The wear test revealed that both the wear performance and coefficient of friction (COF) were improved after FSP. The COF was improved from 0.27461 in base material to 0.22570 in FSPed samples. Surface roughness test showed that the sample with more micro-hardness showed better surface roughness as compared to the other samples.

Keywords Friction stir processing · AA2014 · Al₂O₃ · Surface composites · Micro-hardness · Wear

1 Introduction

Aluminum alloy 2014 (AA2014) is one of the commonly used alloys in areas like aerospace, military equipment, etc. However, due to its low hardness and less wear resistance, the use of AA2014 is limited in the industry. To overcome the limitations, various methods were proposed by various researchers [1–3]. To study hardness property, Dwivedi et al. [4] produced metal matrix composites (MMCs) by using AA2014 and eggshells waste particulates as reinforcement material. Similarly, Durmus et al. [5] used age-hardening on AA2014, whereas Aksoz and Bostan [6] studied the effect of aging and cryo-aging treatment on microstructure and hardness of AA2014–SiC MMCs. Similarly for improving wear behavior, Canakci et al. [7] used an artificial neural network to predict wear behavior of

AA2014/B₄C_p MMCs, whereas Nagral et al. [8] investigated wear behavior of AA2014–ZrO₂ nano-composite by using a two-stage stir casting process. All these studies were conducted to improve the limiting properties of AA2014 alloy. It has been seen that most of the methods included the production of composite material in which some reinforcement particles were added with the AA2014 alloy; but in case of bulk composites, the properties like toughness and ductility also reduce. But if the need is only to enhance the surface properties like hardness and wear, then a new technique in which only the surface of the material is converted into composite could be used. In this way, only the surface composite is made and the remaining surface remains the same as the base material.

Hence to improve the hardness and wear behavior of AA2014 alloy, the production of the surface composite

✉ Shalok Bharti, shalokbharti8@gmail.com | ¹Department of Mechanical Engineering, Institute of Technology, Nirma University, Ahmedabad, Gujarat 382481, India.



is necessary. The surface composite of AA2014 has been produced by various researchers [9–13] by using different techniques like thermal spraying, cast sinter, laser surface engineering, etc. These techniques have their limitations such as producing high temperatures, and toxic fumes. Therefore an environmentally friendly technique was required in which the temperature does not rise much and thus does not melt the base as well as reinforcement material. For this, a new technique called friction stir processing (FSP) was produced by Mishra et al. [14] in 1999. The process is a solid-state process and the surface composite could be easily produced by this technique. This technique was based upon the basic principle of friction stir welding (FSW) which was developed by “The Welding Institute” (TWI) in 1991 [15, 16]. FSP is a thermo-mechanical process in which a rotating tool is plunged into the base material and a traverse speed is provided in the transverse direction so that the friction between tool and surrounding material produces enough heat to make the material into semi-solid state. The stirring action of tool helps to move the material from advancing side of the material to the retreating side of the material producing the surface composite with a uniform dispersion of the reinforcement particles into the base material.

FSP has been used in various practices since the last two decades. Various researchers used this technique over different materials and found enhanced properties and better microstructure. Aluminum, magnesium, copper, etc., are some of the few materials over which FSP has been successfully applied [17–19]. Mazaheri et al. [20] studied the tribological effect of FSP on AZ31 magnesium alloy and found that the ZrO_2 reinforcement particles helped to enhance the hardness as well as wear resistance of the material. Suganeswaran et al. [21] studied FSP on Al7075 alloy and found that the reinforcement particles helped to produce fine grained microstructure with enhanced wear resistance. Naghshekish et al. [22] investigated the effect of graphene oxide reinforcement particles on Al5083 using FSP. They observed that the FSP helped to improve the strength of the material and produced fine-grained microstructure. Senthil and Balasubramanian [23] studied FSP on LM25AA using 10% SiC powder. They found that the threaded cylindrical tool pin produced the homogeneous dispersion of the reinforcement particles and helped to enhance the hardness of the material. Similarly various researchers used FSP technique to enhance the microstructure and properties of the material.

Surface composite of AA2014 was prepared by using various reinforcement particles. Sharma et al. [24] studied the effect of FSP on AA2014/SiC surface composite by using a rotating speed of 710 rpm and a traverse speed of 100 mm/min. They produced surface composite with better microstructural grain refinement, but hardness

property was reduced in their study. Similarly, John et al. [25] studied the effect of FSP on AA2014 by using a rotating speed of 600–1400 rpm and a traverse speed of 30–90 mm/min. They used tools with different pin profiles and found increased hardness and better grain refinement after the process. Satyanarayana and Kumar [26] performed multi-pass FSP on AA2014 and post-heat treatment was applied over its surface to improve its mechanical properties. They found that the properties of the heat-treated FSPed samples were enhanced after the process. In the same way, John et al. [27] investigated the effect of various process parameters (like feed, spindle speed, tool pin profile, and tool tilt angle) on the surface of AA2014–T6 alloy by using Taguchi’s technique. They studied different mechanical properties like tensile strength and found that the tool with hexagonal pin profile provided maximum enhanced properties. In most of the previous studies, researchers used FSP to refine the microstructure and enhance the mechanical properties of the material. But the effect of FSP on mechanical, tribological and microstructural properties of AA2014 has not been wholesomely investigated. The objective of this study is to produce AA2014/ Al_2O_3 surface composite by FSP and study its effect on micro-hardness, microstructure and tribological properties. For this, the constant tool traverse speed of 40 mm/min was used, whereas two tool rotating speeds of 1000 and 1400 rpm were used for the process. The prepared surface composite was investigated for its microstructure using optical microscopy, micro-hardness by Vickers hardness tester, and wear property on pin-on-disk tribometer. Surface roughness test for the prepared surface composite was also studied. The prepared surface composite by FSP showed better micro-hardness and wear resistance as compared to the as-received AA2014.

2 Experimental procedure

2.1 Materials

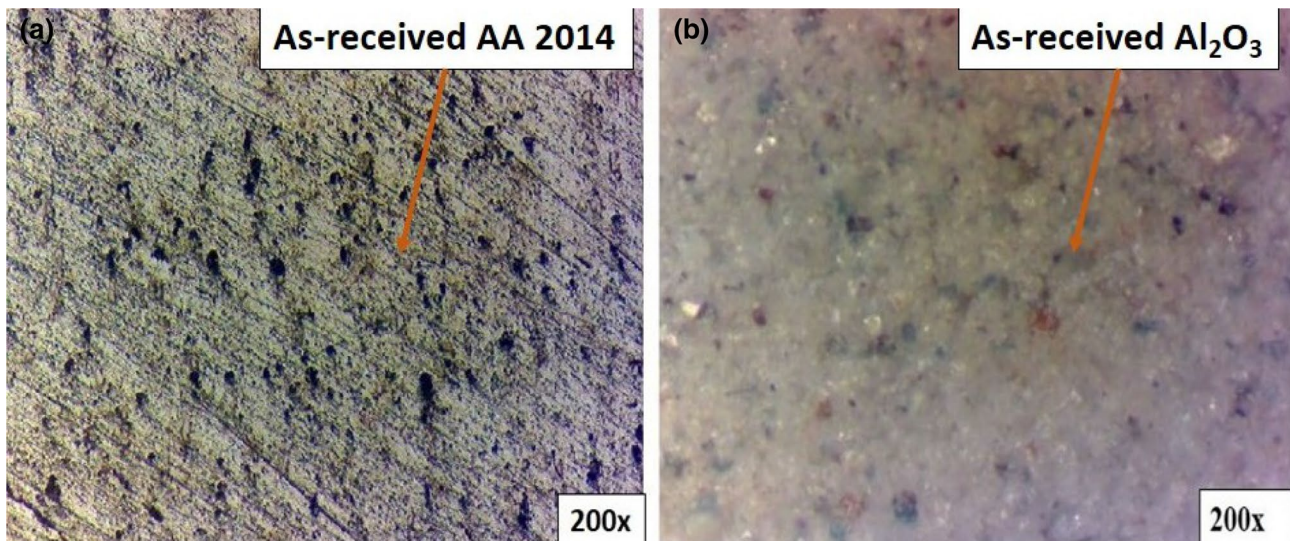
In this study, aluminum 2014–T4 alloy (AA2014) having 5 mm thickness, 300 mm length, and 54 mm width was used as the parent material for the fabrication of surface composite. Table 1 shows the chemical composition of as-received AA2014. Aluminum oxide (Al_2O_3) with the average grain size of 15 μm was used as the reinforcement material. Figure 1 shows the optical microscopy of the used AA2014 and Al_2O_3 .

2.2 Sample processing

The experimental setup used for the process is shown in Fig. 2. A simple vertical head milling machine was used

Table 1 Chemical composition of AA2014

	Cu	Si	Mg	Cr	Mn	Al
wt%	~4.4	~0.8	~0.5	~0.10	0.6 max	Balance

**Fig. 1** Optical Microscopy of **a** as-received AA2014 and **b** as-received Al₂O₃ at 200× magnification**Fig. 2** FSP experimental setup

for the process. Clamping was used to hold the workpiece over the bed of the machine so that workpiece does not experience any vibration or displacement during the process. A combination of two rotating speeds of 1000 rpm and 1400 rpm and one traverse speed of 40 mm/min was used for the process. All the samples were processed with a tool tilt angle of 1 degree and a constant tool traverse speed of 40 mm/min. To insert the Al₂O₃ reinforcement particles into the AA2014, the hole method was used in the process. To prevent agglomeration and clustering of

reinforcement particles, the zigzag hole pattern was made. A total of 17 holes were drilled into the AA2014. Holes with a diameter of 3 mm and depth of 2 mm were drilled by using CNC vertical milling machine. Figure 3 shows the hole pattern in the workpiece.

The volume fraction and weight percent of the reinforcement particles were estimated as follows:

- (i) Stir zone volume:

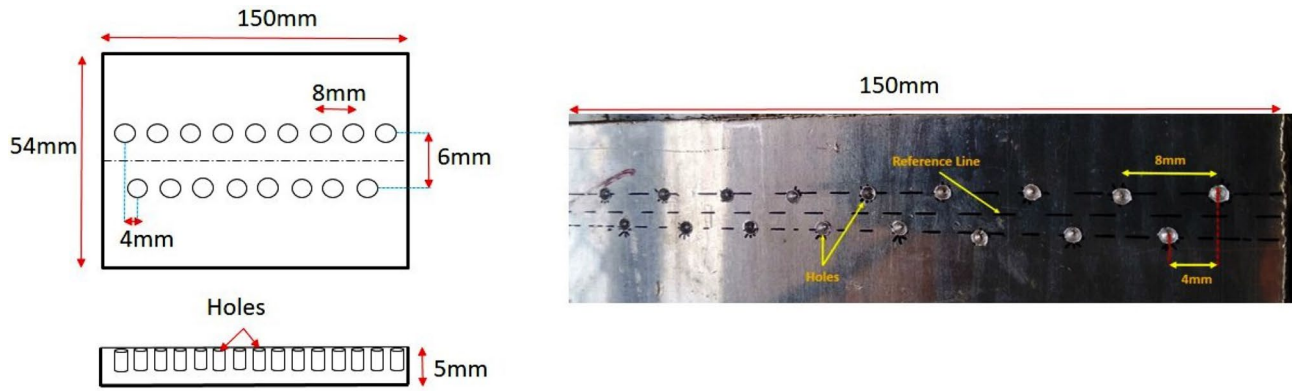


Fig. 3 Hole pattern in the AA2014 workpiece

$$V_{SZ} = \text{pin diameter (4 mm)} \times \text{advancing distance (150 mm)} \times \text{depth (4 mm)} = 2400 \text{ mm}^3 \quad (1)$$

(ii) Individual hole volume:

$$V_H = \text{hole area } (\pi(2)^2/4 \text{ mm}^2) \times \text{hole depth (3 mm)} = 9.43 \text{ mm}^3 \quad (2)$$

(iii) The volume of the matrix:

$$V_M = V_{SZ} - 17 \times V_H = 2239.69 \text{ mm}^3 \quad (3)$$

(iv) The volume fraction of the particles:

$$V_f = (17 \times V_H) / V_{SZ} = 6.68\% \quad (4)$$

(v) Matrix weight:

$$W_M = V_M \times \rho_{(AA2014)} = 6.27 \text{ g} \quad (5)$$

(vi) Reinforcements weight:

$$W_R = 17 \times V_H \times \rho_{(Al_2O_3)} = 0.63 \text{ g} \quad (6)$$

(vii) The weight percent of the particles:

$$\text{Wt}\% = W_R / (W_M + W_R) = 9.13\% \quad (7)$$

The density of AA2014 and Al_2O_3 is 2.82 and 3.95 g/cm^3 , respectively. It should be noted that the real weight percent of the reinforcement particles is lower than the calculated percentage. It is due to the presence of the porosities between the reinforcement particles [20, 28].

Hardened H13 steel was used as the tool material. The taper cylindrical pin profile was used for the pin. The tool has a shoulder diameter of 18 mm, a pin diameter of 4 mm, and a pin length of 4 mm. Figure 4 shows the FSP tool and its dimension. The reinforcement particles were mixed with the acetone to make a paste of reinforcement and

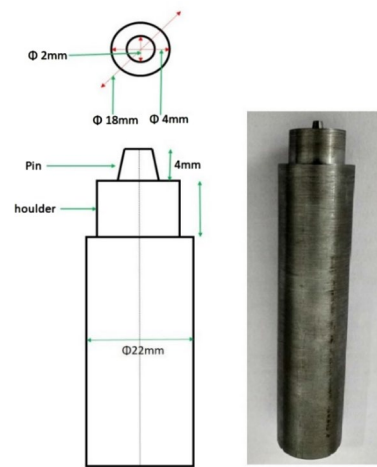


Fig. 4 FSP tool and its dimension

were then inserted into the holes. This was done to avoid the spreading of reinforcement particles during processing. After inserting Al_2O_3 reinforcement particles into the holes, a pinless tool was used to pack the particles into the holes, whereas the tool with pin was used for the actual processing. The schematic of process steps for developing the surface composite of AA2014/ Al_2O_3 is shown in Fig. 5. Single-pass FSP was used to perform FSP in this study. A total of three samples were obtained from the experiment. The first sample was that of the sample with a tool rotating speed of 1000 rpm (sample A). The second sample was that of the sample with a tool rotating speed of 1400 rpm (sample B), whereas the third sample was that of the as-received AA2014 alloy (sample C).

2.3 Characterizations

To prepare the samples for microstructure analysis, the samples were firstly grounded using the emery papers

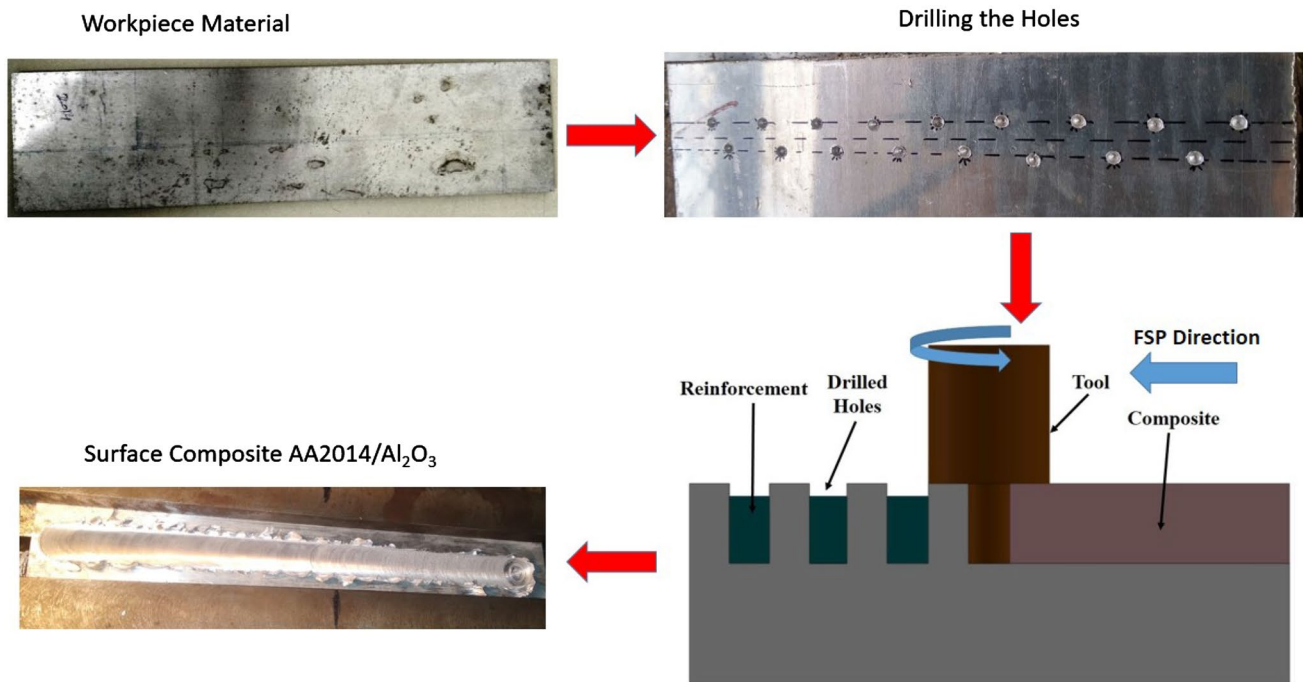


Fig. 5 Mechanism of producing surface composites by FSP

ranging from 100 to 2000 grade. After that, the samples were further polished in a double-disk polishing machine using a diamond polishing paste of 3 μm size. To investigate the microstructure of the prepared samples, Keller reagent (distilled Water—190 ml, nitric acid—5 ml, hydrochloric acid—3 ml, hydrofluoric acid—3 ml) etchant was used. Optical microscopy was used to observe the microstructure of the samples. The samples were cut from the cross section as well as the transverse section area.

To analyze the effect of FSP on the mechanical property of the material, the micro-hardness of samples were measured. The micro-hardness of the prepared samples was measured using Vickers micro-hardness tester using a load of 200 g for a dwell period of 15 s. The samples for the micro-hardness test were taken from the cross-section as well as the transverse section of the samples.

To test the surface integrity of the FSPed samples, a surface roughness test was conducted. The test was conducted on Mitutoyo surface roughness tester having a resolution of 0.01 μm . The evaluation length was 5 mm for the test.

To investigate the effect of FSP on the tribological properties of the material, wear tests of the samples were measured. The wear test was performed on the pin-on-disk tribometer. The wear test was performed at room temperature. The test was accomplished by using the load of 10 N, the sliding distance of 1000 m, and track diameter of 80 mm parameters. Mass losses of the samples were

measured before and after the test using a digital weighing machine with the least count of 0.001 g. The coefficient of friction was measured continuously against the sliding distance. A reading of wear versus time has also been noted during the test. Figure 6 shows the different samples and their cutting position in the FSPed region.

3 Results

3.1 Parameter optimizing

The optimum combination of tool traverse speed and tool rotating speeds helps in the easy flow of the material from the advancing side toward the retreating side of the plate [29–31]. By increasing the traverse speed, time taken for the processing is less due to which less heat is generated, and thus the grain growth is limited in this case, whereas with decreasing traverse speed the contact time between tool and material is more which results in grain softening and thus increased grain size. Similarly increasing rotating speed helps to generate more heat, and decreasing rotating speed produces less heat. Therefore for a defect-free sample, the optimum combinations of rotating as well as traverse speed are required. The values of the optimum speed parameters were selected based upon the literature review [32–37]. Thus the rotating speed of 1000 and 1400 rpm and constant tool traverse speed of 40 mm/min were chosen for the experiment. The combination helped

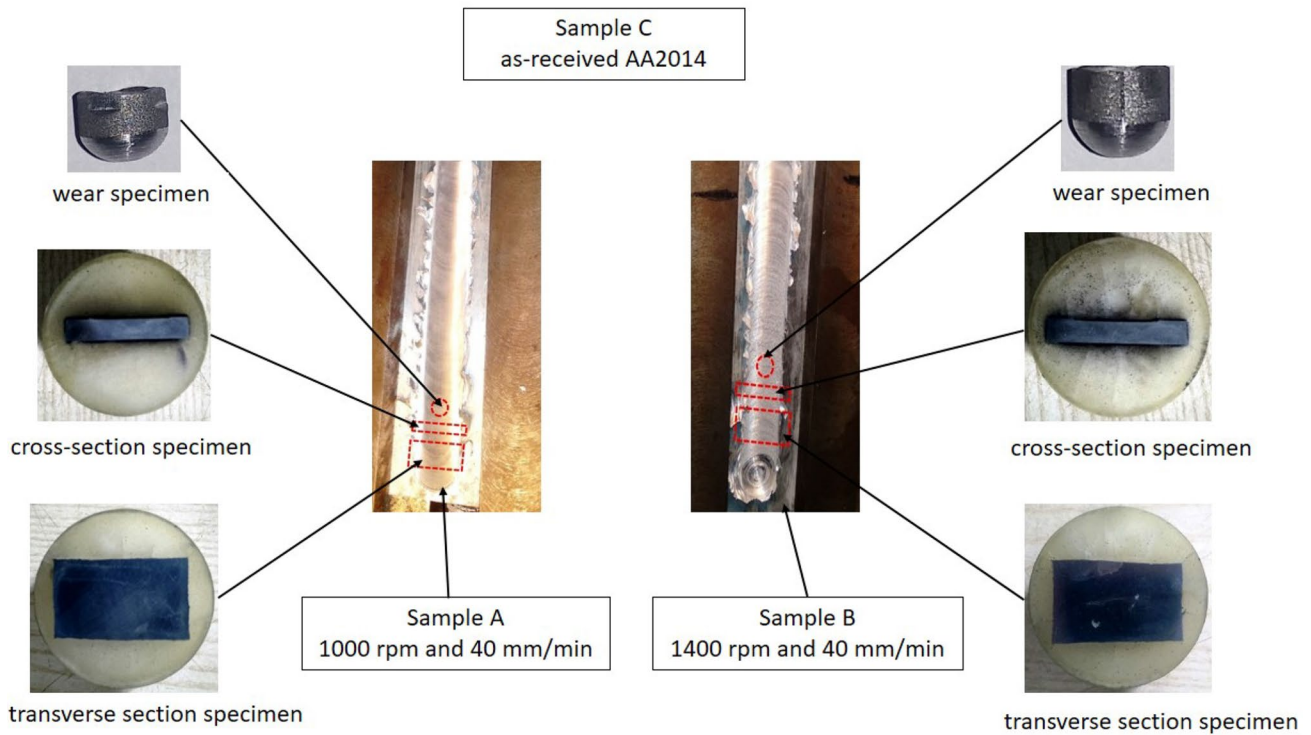


Fig. 6 Different samples from FSPed region

the process to produce a defect-free surface composite with good surface appearance.

3.2 Microstructural analysis

The microstructural analysis of the transverse and cross-section samples was analyzed using the Optical Microscope with an image analyzer. The samples were etched with Keller’s reagent. The samples were examined at 50×, 100×, 200×, 500× and 1000× magnification, but the best view was observed at 200× and 500× magnification. The

grain size was measured by line interception method using 10 number of lines at 1° and 100 threshold using ASTM E112/E1382-91 standard. FSP helped to reduce the average grain size of the FSPed samples. Figure 7a and b shows the optical microscopy of the base material with the average grain size of ~ 21.9 μm. The average grain size of ~ 9.2 μm was observed in sample A, whereas with the increase in the tool rotating speed, the average grain size was further reduced ~ 3.8 μm in sample B. Table 2 shows the average grain size of each sample. It should be noted that each grain size is an average of sixteen readings taken

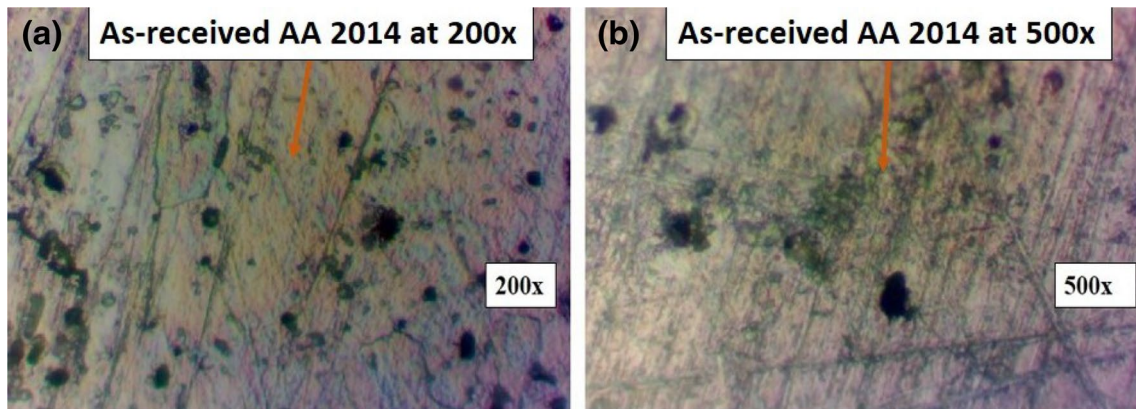
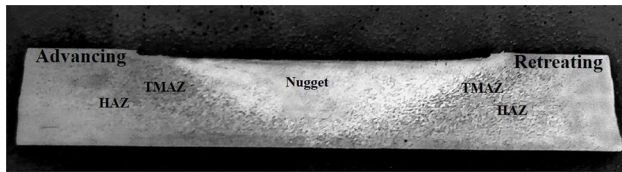


Fig. 7 Optical micrographs of base material (AA2014) a at 200× b at 500×

Table 2 Average grain size for each sample

Sample	Rotating speeds at constant 40 mm/min traverse speed	Average grain size (μm)
Sample A	1000 rpm	~ 9.2
Sample B	1400 rpm	~ 3.8
Sample C	As-received	~ 21.9

**Fig. 8** Nugget and other zones produced after FSP (FSPed sample at 1400 rpm speed)

from the FSPed region. Figure 8 shows the different nugget and other zones of sample B with tool rotating speed of 1400 rpm and traverse speed of 40 mm/min produced by FSP, whereas Fig. 9 shows the transition zone from the coarser grains in the unprocessed zone to the refined grains in the processed zone in AA2014/ Al_2O_3 surface composite at different rotating speeds. The nugget zone and transition zone help to observe the flow region from where the grain size changed from coarser to finer. It also helps in determining the processed region. The distribution of Al_2O_3 reinforcement powder can be seen in Fig. 10 for different processing conditions. The presence of the Al_2O_3 can be seen as the white particles in the microstructure. The presence of Al_2O_3 reinforcement particles helped to increase various properties in the FSPed region as compared to the base material.

From the microstructure analysis, it was observed that FSP helped in the dispersion of the Al_2O_3 reinforcement particles into the base material. The difference in the tool rotating speed affected the microstructure of the FSPed samples. With the increase in the tool rotating speed, the grains were more refined as compared to the low tool rotating speed. The average grain size was reduced from $\sim 21.9 \mu\text{m}$ in base material to $\sim 9.2 \mu\text{m}$ in 1000 rpm sample and further $\sim 3.8 \mu\text{m}$ in 1400 rpm sample, which clearly states that with the increase in the tool rotating speed, the average grain size of the sample reduces. In some studies [38–40], clustering and agglomeration were found during the processing, but no major clustering

or agglomeration was observed during the present investigation.

During FSP, the high amount of friction leads to the heat generation which produces severe plastic deformation into the FSPed region. Thus the dynamic recrystallization takes place after the FSP [41]. Due to the continuous plastic deformation in the nugget zone, the dynamically recrystallized grains were produced which helped to reduce the grain size in the FSPed region [41, 42]. It has been observed that the grain growth in the FSP region was reduced due to the presence of Al_2O_3 reinforcement particles which form the pinning effect and thus act as the barrier for the growth and movement of the grains [43]. It has also been observed that the Al_2O_3 particles were more uniformly distributed in sample B with 1400 rpm rotating speed. It is due to the reason that the increase in rotating speed leads to the generation of optimum heat which softens the region and helps in easy movement of the reinforced particles and hence reduces the chance of agglomeration.

3.3 Micro-hardness

Micro-hardness test was performed to understand the effect of tool rotating speed on the micro-hardness of FSPed surfaces. AA2014 was processed using two different tool rotating speeds with Al_2O_3 as reinforcement powder. Micro-hardness of the samples was measured using “Vickers micro-hardness tester”. The tests were conducted in transverse as well as cross-section surface. In the case of the transverse section, the indentation was made on the surface of the material, whereas in the case of a cross-section area the indentation was made at 1 mm below the surface of the material. During the investigation, it was observed that the FSP helped to enhance the micro-hardness values in both the samples A and B. Table 3 shows the micro-hardness on the surface with indentation figures for the samples A, B, and C. Figure 11a shows the surface micro-hardness plot of the FSPed sample from the top surface (transverse section) of the FSPed Sample. It was observed that the maximum hardness values were observed in the nugget zone of the sample. The hardness values gradually increased from both advancing side and retreating side and were maximum at the center of the nugget zone. The average micro-hardness of the base material (BM) was found to be 118 Hv. FSPed sample “B” showed better micro-hardness as compared to the FSPed Sample “A”. The maximum of 147 Hv micro-hardness value was obtained in sample B, whereas in sample A,

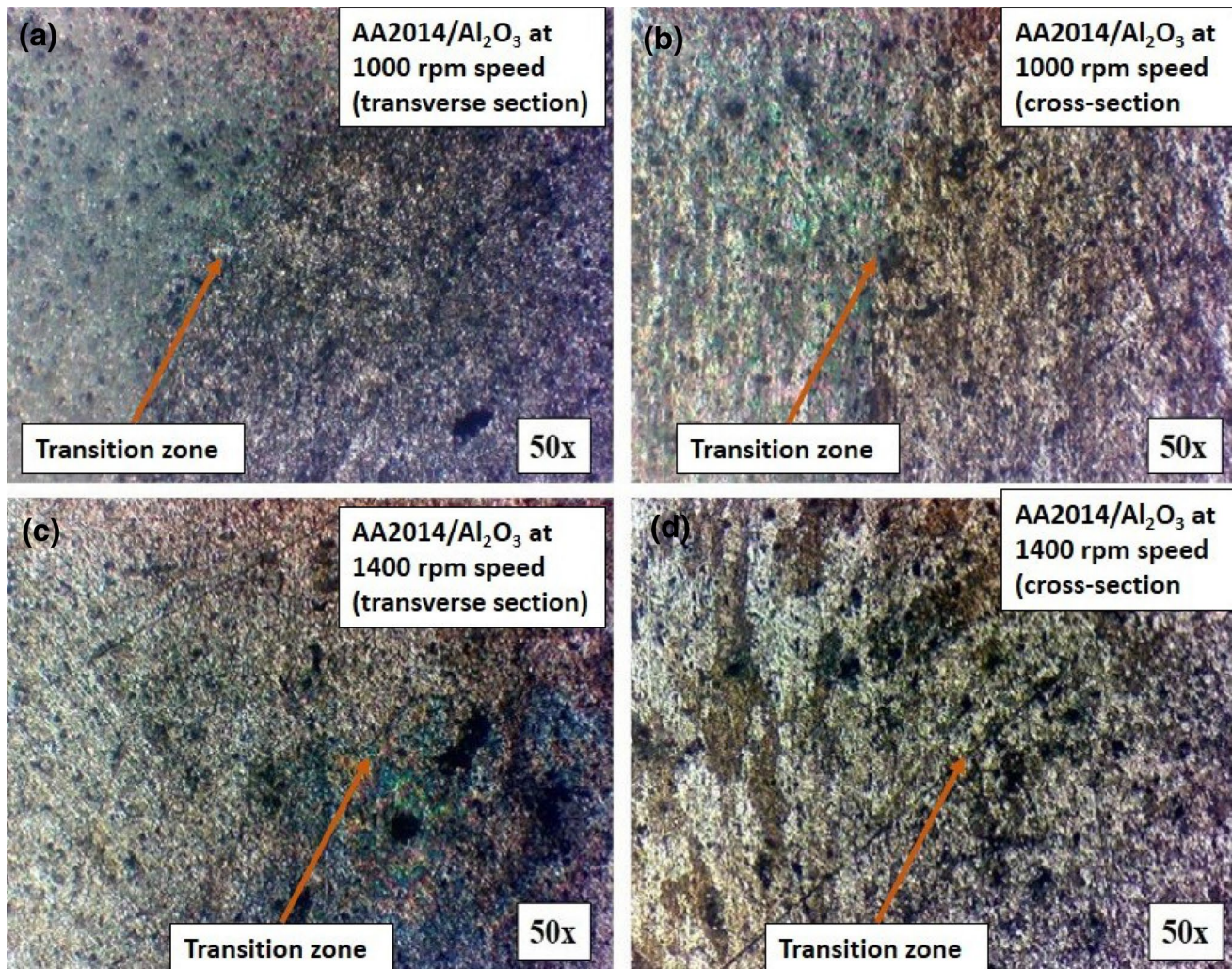


Fig. 9 Transition zone (a) sample A at transverse section, (b) sample A at cross section, (c) sample B at transverse section (d) sample B at the cross section

the maximum micro-hardness value was observed to be 142 Hv. Figure 11b shows the micro-hardness plot from the cross-section surface of the FSPed sample. These observations are similar to those in the transverse section. However in this section a sudden increase in hardness values for both samples A and B were observed in advancing side and retreating side. In the cross-section area, sample B showed a maximum of 154 Hv micro-hardness value whereas sample A showed a maximum micro-hardness value of 143 Hv.

It was observed that with the increase in rotating speed the micro-hardness of material was increased. It is observed that the tool rotating speed of 1400 rpm showed better micro-hardness value as compared to the tool rotating speed of 1000 rpm. According to the Hall–Petch equation, the hardness property of the material increases with the refinement in the grain size because of the grain boundary strengthening mechanism [43]. And we observed in the microstructure analysis that sample B showed finer grain size as compared to the sample A.

Therefore enhanced micro-hardness in sample B was observed as compared to the sample A. In sample B, due to the high rotating speed and better grain refinement, the reinforcement particles were dispersed more homogeneously and therefore showed better micro-hardness value as compared to the sample A. It was also observed that the cross-section area showed more micro-hardness value as compared to the transverse section due to the reason that the cross-section samples have higher reinforcement particle concentration as compared to the transverse section. The results are in agreement with the Harati et al. [44] who observed that the FSPed samples with fine grain size showed better micro-hardness values as compared to samples with coarser grain size. The results are also in the agreement with Khan et al. [45] who studied the effect of FSP on hardness UHMW polyethylene composite and found that the increase in rotating speed helped the composite to increase in its hardness values.

3.4 Surface roughness

The surface quality of the produced surface composite is affected by the surface roughness of the processed workpiece. Process parameter settings affect the surface quality of the processed workpiece in FSP. With the increase in heat generation during FSP, the surface becomes soft and reduces the surface roughness and thus enhances the surface quality, whereas the presence of Al_2O_3 in aluminum matrix increases the roughness which means the aluminum without reinforcement shows less roughness as compared to the reinforced aluminum. From the experiment, it was observed that the FSPed sample with a rotating speed of 1400 rpm showed less surface roughness as compared to the sample with 1000 rpm speed. This is due to the reason that the 1400 rpm sample experienced high heat which softened the surface and a smooth surface was obtained, whereas the 1000 rpm sample experienced less heat and thus more roughness was obtained in this sample. Similar results were observed by Ramezani et al. [46] who studied surface integrity of AA7075/SiC surface composite produced by FSP. They observed that the surface roughness of the FSPed sample reduced with an increase

in rotating speed. They concluded that the increase in rotating speed produces plastic deformation which helps in lower forces and friction. The observed surface roughness values for processed samples in our study are shown in Table 4.

3.5 Wear behavior

3.5.1 Wear rate

The mass loss of samples A, B, and C before and after the wear test at a sliding distance of 1000 m under a normal load of 10 N is shown in Table 5. It was observed that the mass loss of the base material (AA2014) was more as compared to that of the FSPed samples. The increase in rotating speed and uniform distribution of Al_2O_3 particles helped the FSPed samples to decrease the mass loss during the wear test.

It has been observed that sample B showed the least mass loss during the wear test. It occurs due to the increase in the rotating speed which helped to provide better grain refinement, improved micro-hardness, and uniform distribution of Al_2O_3 particles during the process. This phenomenon can be further explained by the Archard's equation which states that the wear rate is inversely proportional to the hardness of the material [47]. Thus improvement in the micro-hardness in sample B improved its wear resistance and thus less mass was lost during the wear test. Also, Al_2O_3 particles are hard particles and are hard to penetrate or perform cutting over their surface by some other counter material like steel disk in our pin-on-disk test.

3.5.2 Coefficient of friction (COF)

The graph for the coefficient of friction (COF) for samples A, B, and C against the sliding distance is shown in Fig. 12. It was observed that the sample A showed a drop in COF initially as compared to sample C. It is due to the reason that the sample A has more hardness value as compared to the sample C which helped the sample A to enhance the wear resistance and thus COF, whereas the lowest COF was observed in sample B which is due to the reason

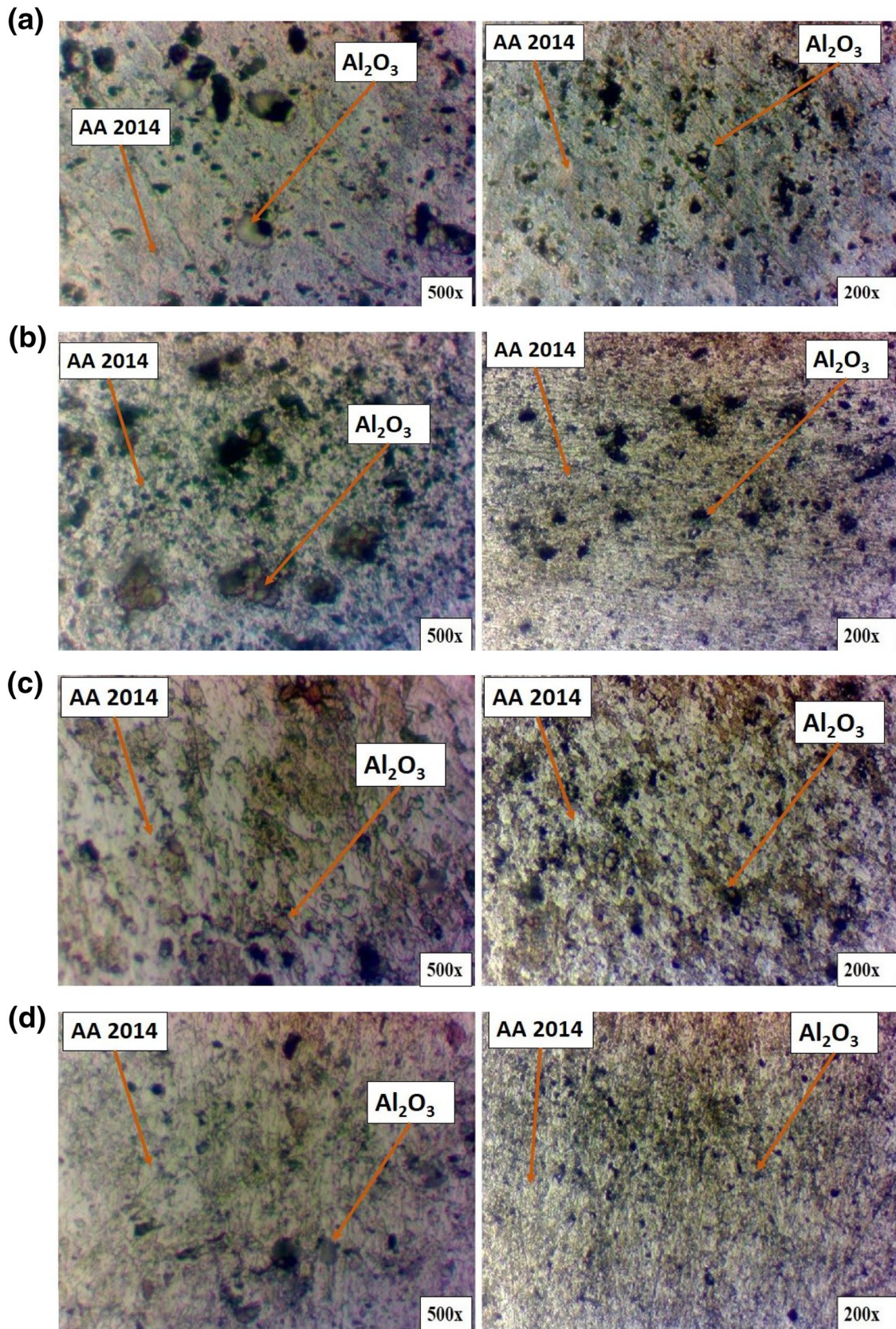
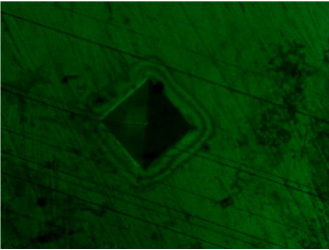
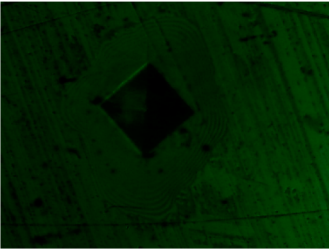
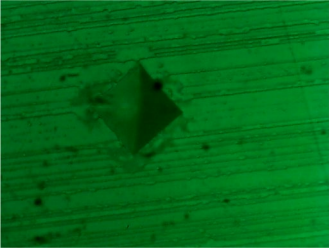


Fig. 10 Distribution of Al₂O₃ powder (a) Cross-section of sample A at 500× and 200× with 1000 rpm speed, (b) transverse section of sample A at 500× and 200× with 1000 rpm speed, (c) cross section of sample B at 500× and 200× with 1400 rpm speed, (d) transverse section of sample B at 500× and 200× with 1400 rpm speed

that sample B showed maximum micro-hardness which helped its surface to experience less COF as compared to other surfaces. In case of sample B due to the high tool rotating speed, more heat was generated in this sample as

Table 3 Maximum micro-hardness on cross-section and a transverse section with indentation figures for the samples A, B and C

Sample	Indentation print (random from readings—for reference)	Average micro-hardness (Hv) before FSP	Micro-hardness (Hv) after FSP (Max.)—cross-section	Micro-hardness (Hv) after FSP (Max.)—transverse section
Sample A-1000		118	143	142
Sample B-1400		118	154	147
Sample C-base material (AA2014)		118	—	—

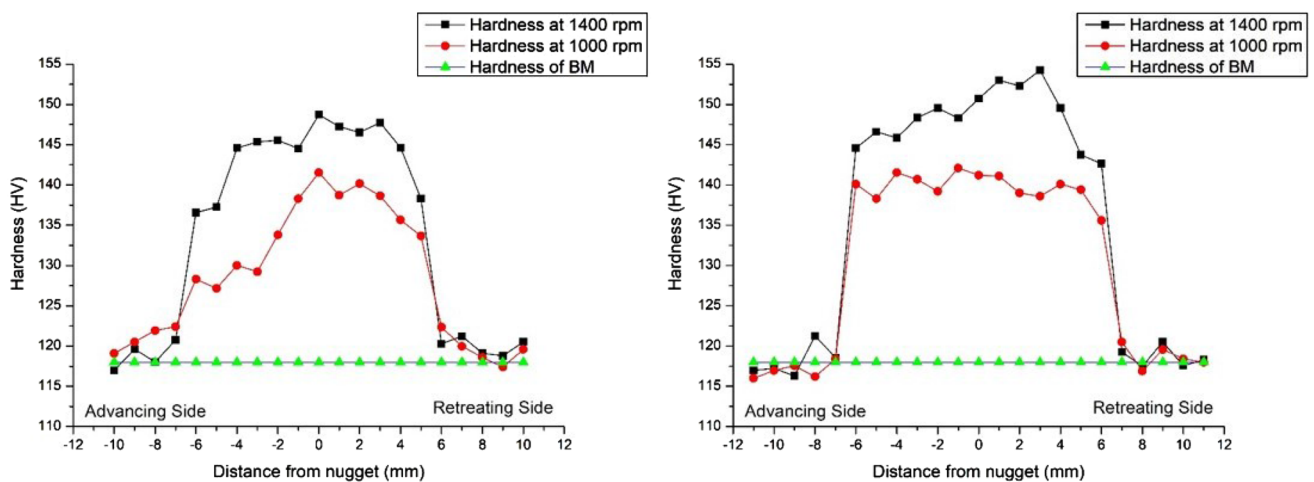


Fig. 11 Micro-hardness plot (a), transverse section (b) Cross-section

Table 4 Surface roughness values for the processed samples

Sample	Rotating speed (constant traverse speed of 40 mm/min)	Reinforcement	Surface roughness (μm)
1	1000	Al_2O_3	8.821
2	1400	Al_2O_3	3.912
3	Base material	Nil	1.218
4	AA2014 (without FSP)	Nil	0.577

Table 5 Mass loss in samples A, B, and C before and after the wear test

	Mass before wear test	Mass after the wear test	Mass difference
Sample A-1000	0.297	0.295	0.002
Sample B-1400	0.331	0.330	0.001
Sample C—as-received aluminum	0.304	0.300	0.004

compared to samples A and C. This heat helped in homogeneous dispersion of the reinforcement particles which further helped to enhance the wear resistance and COF of this sample more than samples A and C. It was observed that sample B due to its high hardness and better microstructure showed minimum COF with an average COF of 0.22570 followed by sample A having an average COF of 0.26974, whereas sample C showed maximum COF with an average COF of 0.27461 during the test. Similar results were found by Vakili-Azghandi et al. [48] who studied FSP on wear resistance and found that the increase in hardness values increased the wear resistance of the material and decreased the COF. The result can also be verified by the results found by Rana and Badheka [49] who studied the FSP and wear behavior of AA7075 alloy. They found that the increase in tool rotating speed helps in uniform distribution of reinforcement particles which further helps in enhanced wear resistance and decreased COF. In our study, similar results were found. With the increase in rotating sample, the hardness as well as COF properties of the material enhanced.

Figure 13 shows the wear graph of samples A, B, and C with respect to time. It has been observed that the wear of samples A, B, and C reduced with an increase in time. But samples A and B due to better microstructure and micro-hardness provide better wear resistance over time. It is observed that sample B showed better wear (average 83.386 μm per unit time) as compared to sample A with

average wear of 112.999 μm per unit time and sample C with average wear of 155.322 μm per unit time due to its improved mechanical as well as microstructural properties. In all graphs, wear firstly increased and then became flattened with an increase in time. This behavior is because the wear samples initially needed to overcome and break the adhesion force between the samples and the steel disk due to which an increase in wear was seen initially in the graph. Also, our test included the dry sliding test which also affects the results. The results are in agreement with the study conducted by Mazaheri et al. [20] who studied FSP and its effect on wear resistance on AZ31 alloy. They found that the enhanced micro-hardness helped to increase the wear resistance of the material with respect to time.

4 Conclusion

In this investigation, aluminum 2014 was used to produce composite over its surface by using Al_2O_3 as reinforcement material. AA2014/ Al_2O_3 surface composite was produced successfully by FSP using combinations with 40 mm/min as traverse speed and two different rotating speeds of 1000 rpm and 1400 rpm. To study the effect of rotating speeds on the properties of AA2014/ Al_2O_3 surface composite, microstructural study by optical microscopy, wear test on pin-on-disk tribometer and micro-hardness test on Vickers micro-hardness tester was investigated. The following conclusions were made from the study:

1. Optical microscopy revealed that FSP helped the material to improve its grain structure and reduce the grain size. The average grain size of AA2014 was calculated to be about 21.9 μm which was reduced to 9.2 μm in FSPed sample with 1000 rpm rotating speed and 3.8 μm in FSPed sample with 1400 rpm rotating speed. FSP also helped in uniform distribution of Al_2O_3 into the base matrix and produced fine-grained AA2014/ Al_2O_3 surface composite.
2. The micro-hardness of the FSPed sample was increased by increasing the rotating speed in FSP. Increased rotating speed helps in the grain refinement and helps the reinforcement particles to disperse more uniformly into the base material. The micro-hardness was improved from 118 Hv in the base material to 154 Hv in the FSPed sample with 1400 rpm rotating speed which means FSP helped to achieve micro-hardness improvement by 30%.
3. The surface roughness of 3.912 and 8.821 was achieved in the FSPed sample with 1400 rpm and

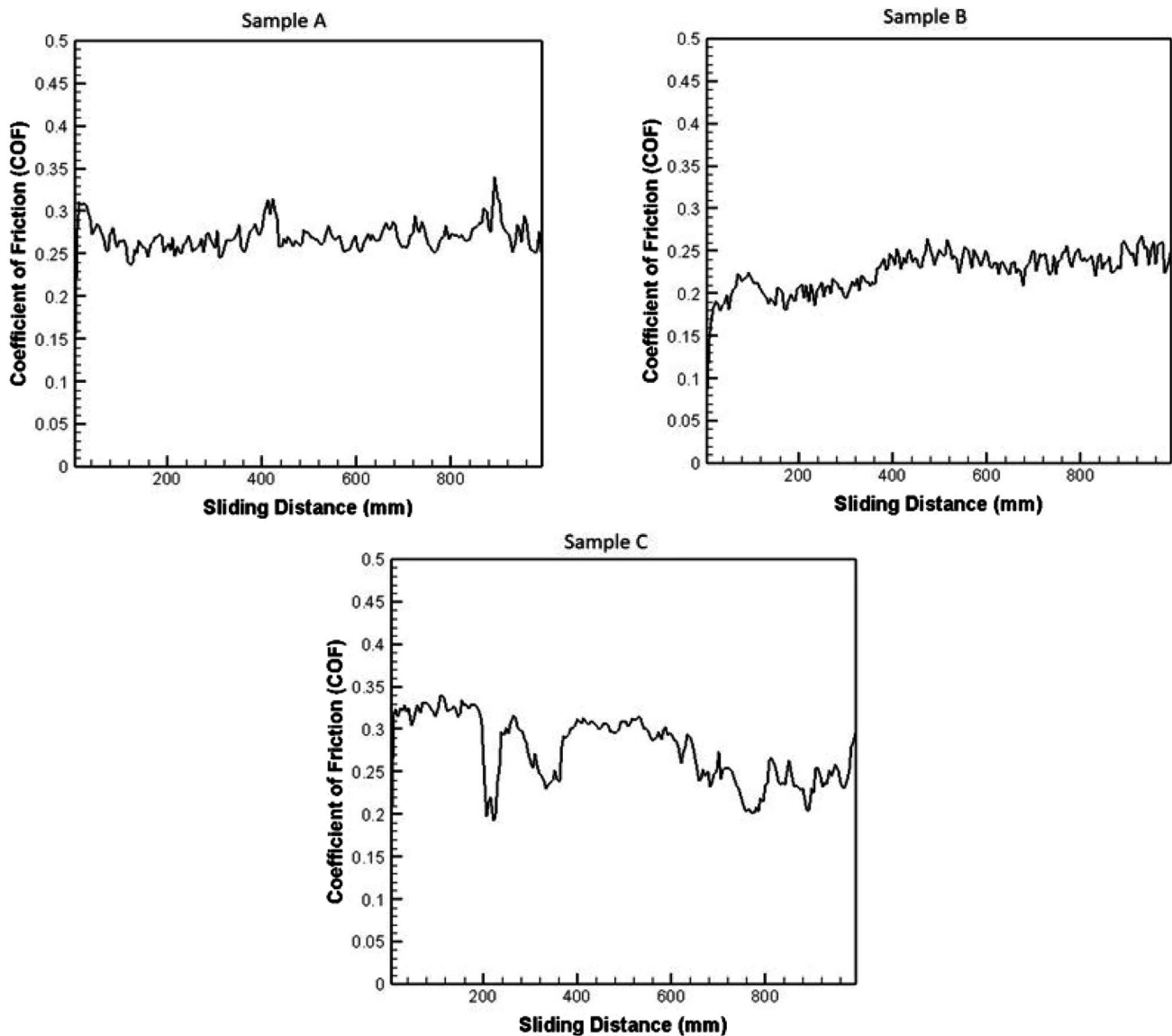


Fig. 12 Deviation in the coefficient of friction with respect to sliding distance for samples A, B, and C

1000 rpm speeds, respectively. The heat generated during the process plays an important role in surface roughness. Also, it was observed that the sample with more micro-hardness showed better surface roughness as compared to others.

- The wear resistance of the material is affected by the presence of Al_2O_3 reinforcement particles and the rotating speed of the FSP. An increase in rotating speed improved the wear resistance of the material from $115.322 \mu\text{m}$ per unit time in base material to $112.999 \mu\text{m}$ per unit time in the FSPed sample with 1000 rpm rotating speed and $83.386 \mu\text{m}$ per unit time in FSPed sample with 1400 rpm rotating speed.

- The average COF was reduced by applying FSP and increasing the rotating speed from 1000 to 1400 rpm. The base material (AA2014) showed an average COF of 0.27461, and the FSPed sample with a rotating speed of 1000 rpm showed COF of 0.26974, whereas the sample with 1400 rpm rotating speed had COF of 0.22570.

These conclusions show that the increase in rotating speed helps to achieve better micro-hardness as well as the wear behavior of the surface composite AA2014/ Al_2O_3 . Increased rotating speed to 1400 rpm and traverse speed of 40 mm/min provide enough heat for grains refinement and uniformly disperse the reinforcement particles into

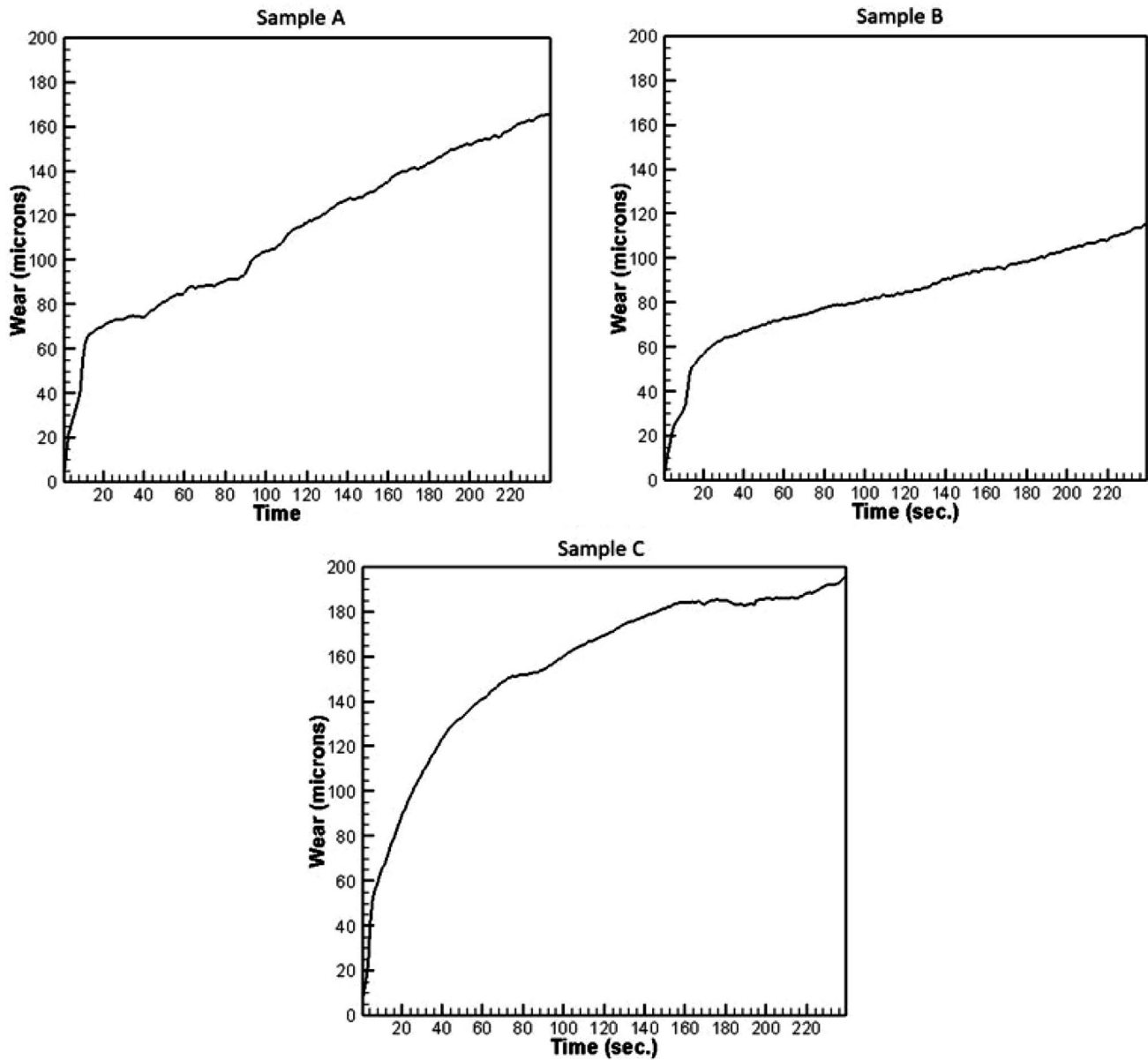


Fig. 13 Deviation in wear with respect to time for samples A, B, and C

the base material. FSP parameters helped to successfully produce a surface composite with enhanced properties and without any defects.

Acknowledgements Authors would like to thank Mr. Arvind Sankhla (Assistant Professor) for providing Al₂O₃ reinforcement particles for the experiment. We also thank Abhijat Joshi, Jayesh Panchal, Dharmendra Naik, and Ramjibhai Patel (Technical Staff) of Department of mechanical engineering, Nirma University, for their help during the experiment.

Author contributions SB was involved in conceptualization, methodology, writing—original draft preparation, NDG was involved in methodology, supervision, review and editing, and KMP was involved in supervision.

Funding This research received no specific grant from any funding agency.

Compliance with ethical standards

Conflict of interest The authors declare that they have no conflicts of interest to report regarding this paper.

References

1. Babu S, Sankar VS, Janaki Ram GD et al (2013) Microstructures and mechanical properties of friction stir spot welded

- aluminum alloy AA2014. *J Mater Eng Perform* 22:71–84. <https://doi.org/10.1007/s11665-012-0218-z>
2. Ureña A, de Salazar JMG, Escalera MD (1996) Diffusion bonding of an aluminium-copper alloy reinforced with silicon carbide particles (AA2014/SiC/13p) using metallic interlayers. *Scr Mater* 35:1285–1293. [https://doi.org/10.1016/1359-6462\(96\)00310-7](https://doi.org/10.1016/1359-6462(96)00310-7)
 3. Babu S, Ram GDJ, Venkitakrishnan PV et al (2012) Microstructure and mechanical properties of friction stir lap welded aluminum alloy AA2014. *J Mater Sci Technol* 28:414–426. [https://doi.org/10.1016/S1005-0302\(12\)60077-2](https://doi.org/10.1016/S1005-0302(12)60077-2)
 4. Dwivedi SP, Sharma S, Mishra RK (2016) Mechanical and metallurgical characterizations of AA2014/eggshells waste particulate metal matrix composite. *Int J Precis Eng Manuf Technol* 3:281–288. <https://doi.org/10.1007/s40684-016-0036-0>
 5. Durmuş HK, Meriç C (2007) Age-hardening behavior of powder metallurgy AA2014 alloy. *Mater Des* 28:982–986. <https://doi.org/10.1016/j.matdes.2005.11.022>
 6. Aksöz S, Bostan B (2018) Effects of ageing and cryo-ageing treatments on microstructure and hardness properties of AA2014–SiC MMCs. *Trans Indian Inst Met* 71:2035–2042. <https://doi.org/10.1007/s12666-018-1336-6>
 7. Canakci A, Ozsahin S, Varol T (2014) Prediction of effect of reinforcement size and volume fraction on the abrasive wear behavior of AA2014/B4Cp MMCs using artificial neural network. *Arab J Sci Eng* 39:6351–6361. <https://doi.org/10.1007/s13369-014-1157-9>
 8. Nagral M, Hiremath V, Auradi V, Kori SA (2018) Influence of two-stage stir casting process on mechanical characterization and wear behavior of AA2014–ZrO₂ nano-composites. *Trans Indian Inst Met* 71:2845–2850. <https://doi.org/10.1007/s12666-018-1441-6>
 9. Dutta Majumdar J, Chandra BR, Nath AK, Manna I (2006) Compositionally graded SiC dispersed metal matrix composite coating on Al by laser surface engineering. *Mater Sci Eng A* 433:241–250. <https://doi.org/10.1016/j.msea.2006.06.105>
 10. Yun E, Lee K, Lee S (2005) Correlation of microstructure with high-temperature hardness of (TiC, TiN)/Ti–6Al–4V surface composites fabricated by high-energy electron-beam irradiation. *Surf Coat Technol* 191:83–89. <https://doi.org/10.1016/j.surfcoat.2004.02.040>
 11. Kang H-K, Kang SB (2006) Thermal decomposition of silicon carbide in a plasma-sprayed Cu/SiC composite deposit. *Mater Sci Eng A* 428:336–345. <https://doi.org/10.1016/j.msea.2006.05.054>
 12. Wang Y, Zhang X, Zeng G, Li F (2000) Cast sinter technique for producing iron base surface composites. *Mater Des* 21:447–452. [https://doi.org/10.1016/S0261-3069\(00\)00036-4](https://doi.org/10.1016/S0261-3069(00)00036-4)
 13. Ding WB, Jiang HY, Zeng XQ et al (2007) The surface modified composite layer formation with boron carbide particles on magnesium alloy surfaces through pulse gas tungsten arc treatment. *Appl Surf Sci* 253:3877–3883. <https://doi.org/10.1016/j.apsusc.2006.08.015>
 14. Mishra RR, Mahoney M, McFadden SS et al (1999) High strain rate superplasticity in a friction stir processed 7075 Al alloy. *Scr Mater* 42:163–168. [https://doi.org/10.1016/S1359-6462\(99\)00329-2](https://doi.org/10.1016/S1359-6462(99)00329-2)
 15. Thomas WM, Nicholas ED, Needham JC et al (1991) GB Patent application no. 9125978.8. *Int Pat Appl* no PCT/GB92/02203
 16. Parikh VK, Badgajar AD, Ghetiya ND (2019) Joining of metal matrix composites using friction stir welding: a review. *Mater Manuf Process* 34:123–146. <https://doi.org/10.1080/10426914.2018.1532094>
 17. Barmouz M, Besharati Givi MK, Seyfi J (2011) On the role of processing parameters in producing Cu/SiC metal matrix composites via friction stir processing: investigating microstructure, microhardness, wear and tensile behavior. *Mater Charact* 62:108–117. <https://doi.org/10.1016/j.matchar.2010.11.005>
 18. Prakash T, Sivasankaran S, Sasikumar P (2015) Mechanical and tribological behaviour of friction-stir-processed Al 6061 aluminium sheet metal reinforced with Al₂O₃/0.5 Gr hybrid surface nanocomposite. *Arab J Sci Eng* 40:559–569. <https://doi.org/10.1007/s13369-014-1518-4>
 19. Luo XC, Zhang DT, Cao GH et al (2019) Multi-pass submerged friction stir processing of AZ61 magnesium alloy: strengthening mechanisms and fracture behavior. *J Mater Sci* 54:8640–8654. <https://doi.org/10.1007/s10853-018-03259-w>
 20. Mazaheri Y, Jalilvand MM, Heidarpour A, Jahani AR (2020) Tribological behavior of AZ31/ZrO₂ surface nanocomposites developed by friction stir processing. *Tribol Int* 143:106062. <https://doi.org/10.1016/j.triboint.2019.106062>
 21. Suganeswaran K, Parameshwaran R, Mohanraj T, Radhika N (2020) Influence of secondary phase particles Al₂O₃/SiC on the microstructure and tribological characteristics of AA7075-based surface hybrid composites tailored using friction stir processing. *Proc Inst Mech Eng Part C J Mech Eng Sci*. <https://doi.org/10.1177/0954406220932939>
 22. Naghshehkeh N, Mousavi SE, Karimzadeh F et al (2019) Effect of graphene oxide and friction stir processing on microstructure and mechanical properties of matrix composite. *Mater Res Express* 6:106566. <https://doi.org/10.1088/2053-1591/ab3a6f>
 23. Senthil V, Balasubramanian E (2020) Effect of tool pin profile on corrosion behavior of friction stir processed LM25AA 10% SiCp metal matrix composites. *Met Powder Rep* 75:110–117. <https://doi.org/10.1016/j.mprp.2019.11.001>
 24. Kumar M, Sharma V, Prakash U et al (2015) Microstructural and mechanical characteristics of AA2014/sic surface composite fabricated by friction stir processing. *Mater Today Proc* 2:2666–2670. <https://doi.org/10.1016/j.matpr.2015.07.229>
 25. John J, Shanmuganatan SP, Kiran MB et al (2019) Investigation of friction stir processing effect on AA2014–T6. *Mater Manuf Process* 34:159–176. <https://doi.org/10.1080/10426914.2018.1532577>
 26. Satyanarayana MVNV, Kumar A (2019) Effect of heat treatment on AA2014 alloy processed through multi-pass friction stir processing. *J Phys Conf Ser* 1240:012077. <https://doi.org/10.1088/1742-6596/1240/1/012077>
 27. John J, Shanmuganatan SP, Kiran MB (2018) Influence and optimization of input parameters on mechanical properties of friction stir processed AA 2014–T6. *Mater Today Proc* 5:25458–25467. <https://doi.org/10.1016/j.matpr.2018.10.351>
 28. Jalilvand MM, Mazaheri Y, Heidarpour A, Roknian M (2019) Development of A356/Al₂O₃ + SiO₂ surface hybrid nanocomposite by friction stir processing. *Surf Coat Technol* 360:121–132. <https://doi.org/10.1016/j.surfcoat.2018.12.126>
 29. Arora HS, Singh H, Dhindaw BK (2012) Composite fabrication using friction stir processing—a review. *Int J Adv Manuf Technol* 61:1043–1055. <https://doi.org/10.1007/s00170-011-3758-8>
 30. Bharti S, Dutta V, Sharma S, Kumar R (2019) A study on the effect of friction stir processing on the hardness of aluminum 6000 series. *Mater Today Proc* 18:5185–5188. <https://doi.org/10.1016/j.matpr.2019.07.517>
 31. Sharma V, Prakash U, Kumar BVM (2015) Surface composites by friction stir processing: a review. *J Mater Process Technol* 224:117–134. <https://doi.org/10.1016/j.jmatprotec.2015.04.019>
 32. Thapliyal S, Dwivedi DK (2018) Barium titanate reinforced nickel aluminium bronze surface composite by friction stir processing. *Mater Sci Technol* 34:366–377. <https://doi.org/10.1080/02670836.2017.1393203>
 33. Luo XC, Zhang DT, Zhang WW et al (2018) Tensile properties of AZ61 magnesium alloy produced by multi-pass friction stir processing: effect of sample orientation. *Mater Sci Eng A* 725:398–405. <https://doi.org/10.1016/j.msea.2018.04.017>

34. Chang CI, Du XH, Huang JC (2008) Producing nanograin microstructure in Mg–Al–Zn alloy by two-step friction stir processing. *Scr Mater* 59:356–359. <https://doi.org/10.1016/j.scriptamat.2008.04.003>
35. Pol N, Verma G, Pandey RP, Shanmugasundaram T (2019) Fabrication of AA7005/TiB₂–B₄C surface composite by friction stir processing: evaluation of ballistic behaviour. *Def Technol* 15:363–368. <https://doi.org/10.1016/j.dt.2018.08.002>
36. Sathiskumar R, Murugan N, Dinaharan I, Vijay SJ (2013) Characterization of boron carbide particulate reinforced in situ copper surface composites synthesized using friction stir processing. *Mater Charact* 84:16–27. <https://doi.org/10.1016/j.matchar.2013.07.001>
37. Sabbaghian M, Shamanian M, Akramifard HR, Esmailzadeh M (2014) Effect of friction stir processing on the microstructure and mechanical properties of Cu–TiC composite. *Ceram Int* 40:12969–12976. <https://doi.org/10.1016/j.ceramint.2014.04.158>
38. Akramifard HR, Shamanian M, Sabbaghian M, Esmailzadeh M (2014) Microstructure and mechanical properties of Cu/SiC metal matrix composite fabricated via friction stir processing. *Mater Des* 54:838–844. <https://doi.org/10.1016/j.matdes.2013.08.107>
39. Khodabakhshi F, Simchi A, Kokabi AH et al (2015) Reactive friction stir processing of AA 5052–TiO₂ nanocomposite: process–microstructure–mechanical characteristics. *Mater Sci Technol* 31:426–435. <https://doi.org/10.1179/1743284714Y.0000000573>
40. Kashani-Bozorg SF, Jazayeri K, Rusop M, Soga T (2009) Formation of Al/B₄C surface nano-composite layers on 7075 Al alloy employing friction stir processing. In: *AIP Conference Proceedings AIP*, pp 715–719
41. Chang CI, Wang YN, Pei HR et al (2006) On the hardening of friction stir processed Mg–AZ31 based composites with 5–20% nano-ZrO₂ and Nano-SiO₂ particles. *Mater Trans* 47:2942–2949. <https://doi.org/10.2320/matertrans.47.2942>
42. Asadi P, Faraji G, Masoumi A, Besharati Givi MK (2011) Experimental investigation of magnesium-base nanocomposite produced by friction stir processing: effects of particle types and number of friction stir processing passes. *Metall Mater Trans A* 42:2820–2832. <https://doi.org/10.1007/s11661-011-0698-8>
43. Lee CJ, Huang JC, Hsieh PJ (2006) Mg based nano-composites fabricated by friction stir processing. *Scr Mater* 54:1415–1420. <https://doi.org/10.1016/j.scriptamat.2005.11.056>
44. Harati F, Shamanian M, Atapour M et al (2019) The effect of microstructure and texture evolution on the hardness properties of the cold rolled AA7075–T6 aluminum alloy during the friction stir processing. *Mater Res Express* 6:046559. <https://doi.org/10.1088/2053-1591/aafe48>
45. Khan I, Hussain G, Al-Ghamdi KA, Umer R (2019) Investigation of impact strength and hardness of UHMW polyethylene composites reinforced with nano-hydroxyapatite particles fabricated by friction stir processing. *Polymers* 11:1041. <https://doi.org/10.3390/polym11061041>
46. Molla Ramezani N, Davoodi B, Farahani M, Khanli AH (2019) Surface integrity of metal matrix nanocomposite produced by friction stir processing (FSP). *J Braz Soc Mech Sci Eng* 41:503. <https://doi.org/10.1007/s40430-019-2014-2>
47. Archard JF (1953) Contact and rubbing of flat surfaces. *J Appl Phys* 24:981–988. <https://doi.org/10.1063/1.1721448>
48. Vakili-Azghandi M, Roknian M, Szpunar JA, Mousavizade SM (2020) Surface modification of pure titanium via friction stir processing: microstructure evolution and dry sliding wear performance. *J Alloys Compd* 816:152557. <https://doi.org/10.1016/j.jallcom.2019.152557>
49. Rana H, Badheka V (2019) Elucidation of the role of rotation speed and stirring direction on AA7075–B₄C surface composites formulated by friction stir processing. *Proc Inst Mech Eng Part L J Mater Des Appl* 233:977–994. <https://doi.org/10.1177/1464420717736548>

Publisher's Note Springer Nature remains neutral with regard to jurisdictional claims in published maps and institutional affiliations.